Milkweed scaffold: A new candidate for bone cell growth

Simon Soulié[a,b,c], Ibrahim Bilem[a,b], Pascale Chevallier[a,b], Saïd Elkoun[d], Mathieu Robert[d], Nicolas Naudé[a,c], and Gaétan Laroche[a,b]

[a]*Laboratoire d'Ingénierie de Surface, Centre de Recherche sur les Matériaux Avancés, Département de génie des mines, de la métallurgie et des matériaux, Université Laval, 1065, avenue de la Médecine, Québec G1V 0A6, Québec, Canada*
[b]*Centre de recherche du CHU de Québec, Hôpital St François d'Assise, 10, rue de L'Espinay, Québec G1L 3L5, Québec, Canada*
[c]*LAPLACE, Université de Toulouse, CNRS, INPT, UPS, France*
[d]*Carrefour d'innovations en technologies Écologiques (CITÉ), Université de Sherbrooke, Sherbrooke, J1K 2R1, Québec, Canada*

ABSTRACT
This study aims to evaluate the potential of milkweed as potential candidate to construct biodegradable scaffold for bone regeneration. A mat made of milkweed, polyethylene, and polypropylene was treated with an atmospheric pressure plasma to functionalize the surface of the polymer assembly with carboxylic acid groups, which enable to conjugate bioactive molecules, while accelerating the degradation of milkweed. Degradation tests demonstrated substantial decrease of the weight of the treated polymer mat as compared to untreated one. Biological assays revealed that the polymer assembly promoted preosteoblast MC3T3 cells recruitment with a significant enhancement observed on the RGD-grafted polymer mat.

KEYWORDS
Asclepias syriaca L., milkweed, bone cell growth, atmospheric pressure plasma.

CITATION
Soulié, S., Bilem, I., Chevallier, P., Elkoun, S., Robert, M., Naudé, N., & Laroche, G. (2019). Milkweed scaffold: a new candidate for bone cell growth. International Journal of Polymeric Materials and Polymeric Biomaterials, 1-12.

This is the author's version of the original manuscript. The final publication is available at Tandof Link Online via https://doi.org/10.1080/00914037.2019.1626391

1 INTRODUCTION

Bone and cartilage regeneration by autogenous cell/tissue transplantation is one of the most promising techniques in orthopedic surgery and biomedical engineering. In bone-tissue engineering applications, a scaffold should meet several criteria, such as a good capacity to interact with the surrounding host tissue. It should also have a high porosity, an interconnected pore network as well as adequate mechanical properties to support cell adhesion, proliferation and differentiation [1]. At the same time, its degradation rate should be balanced with the growth and maturation of neo-formed tissue.

During the last decades, tissue engineering has experienced a strong worldwide expansion since a large scientific community believes that this approach paves the way towards the development of smart materials capable to restore physiological functions of damaged tissues. In general, tissue engineering involves the use of highly porous, three dimensional (3D) and biodegradable scaffolds, which somewhat mimic the natural extracellular matrix. To date, many materials, from a synthetic or

natural source, have been used to create tissue-engineered products [2]. For example, silk-based materials have been explored in bone tissue reconstruction due to their tunable mechanical properties, acceptable biocompatibility, controllable degradability and versatile design [3]. However, it has been highlighted that silk-based materials may trigger an inflammatory response both in vitro and in vivo, due to the presence of sericin in the native silk, known to cause hypersensitivity [4, 5]. In addition, the production of natural silk at an industrial scale is still very laborious, which limits the extent of this material in the biomaterials market [5].

In this study, milkweed fiber was explored to exploit its properties for use as bone scaffold. Very recently, this natural fiber attracted media attention, mainly for its use as thermal insulation in winter clothing [4, 5]. For an identical weight, these fibers are twice warmer than bird fluff. However, the interesting properties of milkweed fibers are not limited to its thermal characteristics [6]. They are also excellent as acoustic insulators, they are hydrophobic and absorb twice as much oil as the existing materials on the market in case of oil spill [7, 8].

Milkweed fiber, like silk, also has adequate biological and mechanical properties to be used as a temporary substitute material in the human body. However, despite an extensive literature review, it turned out that milkweed fiber has never been investigated for tissue engineering applications. Hence, the thick, white sap secreted by the milkweed plant when punctured was shown to contain steroids called cardenolides, which exhibit cardiotonic properties that produce many of the milkweed health benefits. In addition, the milkweed sap has been used externally in numerous traditional medicine practices to treat conditions such as skin ulcers, eczema, tumors, sores and wounds, leprosy, burns, warts, throat and ear inflammation, rheumatism, and headaches [9]. Although cellulose-based materials were already investigated for tissue engineering applications, the milkweed fiber itself has never been the subject of any research in this field.

Because cellulose is not readily degradable by the human body, milkweed must be functionalized to initiate its degradation [10] and provide specific functional groups for biomolecule grafting. One common approach is to functionalize biomaterial surfaces with extra cellular matrix derived peptides able to recruit cells and dictate their behaviors, such as adhesion, proliferation, migration and differentiation. In this work, RGD peptide, which is one of the most documented peptides as the shortest sequence responsible for cell adhesion, will be used to enhance cells recruitment and interactions with milkweed fiber [11]. To allow the grafting of this peptide, cold plasmas processes can be used to create specific chemical groups on the surface of milkweed fiber without damaging its structure [12].

Cold plasmas generate a high density of free radicals through the dissociation of molecules by collision and photochemical processes that allow them to interact with a material. As a result, new chemical species are formed on the surface of fibers and polymers [13]. Thus, cold plasma makes possible to the grafting of molecules onto the material surface. The depth of the modification by plasma treatment is a few tens of nanometers. In this context, cold plasmas processes can be used to modify the outermost layer of materials without modifying their bulk properties [14].

For the purpose of this study, synthetic polymer fibers had to be added to the overall scaffold to provide the non-woven textile structure with sufficient fiber cohesion. Essentially, a composite material, made of 30% PE (polyethylene) / PP (polypropylene) (21%/9%) and 70% milkweed was used [15]. First, we evaluated the structure, distribution and organization of milkweed, PE, and PP fibers in the polymer mat. Then, the surface of the polymer mat was functionalized using a Dielectric Barrier Discharge (DBD) plasma at atmospheric pressure for further grafting of adhesion RGD peptide, while promoting the degradation of the natural component of the polymer (cellulose). Finally, the biological relevance of this polymer was investigated by evaluating preosteoblast cells adhesion on untreated and RGD-grafted scaffolds.

2 MATERIALS AND METHODS

N-(3-dimethylaminopropyl)-N-ethylcarbodiimide hydrochloride (EDC), 2-(N-morpholino) ethanesulfonic acid (MES), 4-(2-hydroxyethyl)-1-piperazineethanesulfonic acid (HEPES), silver nitrate ($AgNO_3$), and TWEEN-20 solution (Sigma–Aldrich, Canada) were purchased from Sigma–Aldrich, Canada. The fluorophore-tagged CG-K(PEG3-TAMRA)-GGRGD adhesion peptide (referred to as RGD-TAMRA; MW 1437 g/mol) was synthesized by Genecust, Luxembourg.

2.1 Milkweed fibers dewaxing

The composition of milkweed, grown in the valley of St-Lawrence River, Quebec, Canada, was given in Table 1. These fibers were then transformed into mats composed of 70% milkweed and 30% synthetic fibers [21% polyethylene (PE) / 9% polypropylene (PP)]. The material was provided by Protec-Style (Granby, Canada). The mats were made by carding together milkweed and core shell PP/PE fibers (PE-coated PP fibers) at temperatures ranging between 80°C and 120°C. In these conditions, PE is almost already molten, while PP is still solid. This enables the sticking of all fibers of the mat, which ensures the cohesion of the mat, while also improving mechanical properties, thanks to the presence of PP. The mats were 1.5 cm thick with a density of 100 g/m^2.

Table 1: Chemical composition (%) of Milkweed fibers [16]

Composition	Cellulose	Hemicellulose	Lignin pectin	Ash	Wax	Sugar
Milkweed (%)	44.0	36.0	13.2	1.0	3.1	2.6

The wax covering milkweed fiber has been removed by Soxhlet extraction in acetone for 24 hours. Milkweed fibers were then vacuum-dried for several days and stored in a desiccator until use.

2.2 Mechanical properties of the polymer mat

Ultimate tensile strength and elongation at break were measured under uniaxial tensile load by means of Zwick machine on 35 x 150 mm rectangular samples at a constant crosshead speed of 2 mm/min. The standard deviation was assessed by testing 4 samples.

2.3 Plasma treatment

The plasma reactor used to functionalize the milkweed fibers was developed by AlmaPLUS srl (Plasma Laboratory Unified System, Bologna, Italy). Plasma parameters, including geometrical patterns design, electrical parameters, gas flow and liquid precursor's injection are monitored via a computer-controlled interface. The experimental setup is shown in Figure 1. Briefly, a helium atmospheric-pressure plasma jet was generated in configurations with a dielectric material between the electrodes, also called Dielectric Barrier Discharge (DBD) configuration. The helium flow was directed to the quartz tube with a flow rate of 3 L.min^{-1}. The polymer sample is in a chamber in the ambient air. High-voltage mono-polar square pulses were applied on the powered electrode with variable magnitude, frequency, and pulse width. Typically, the voltage enabled to ignite the discharge ranged between 5 to 7 kV at a frequency of 15 kHz. Helium is 99.999% pure.

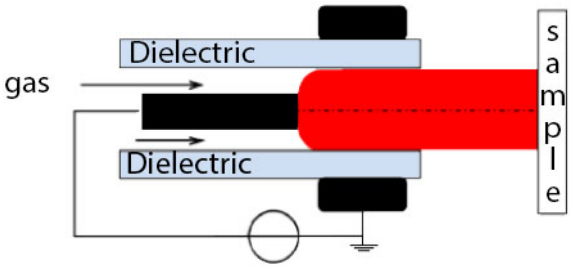

Figure 1. Schematic of the DBD-jet source; the electrodes are represented in black.

Polymer mat samples of 1 x 1.5 cm^2 were introduced under the plasma torch described above. A surface treatment pattern, corresponding to the size of the polymer, was designed using the control software provided with the plasma reactor. The number of passes and the distance between and the sample were adjusted to prevent damages to the fibers while maximizing surface functionalization. Accordingly, it was found that such requirements were reached with a torch-to-sample distance of 20 mm, with a torch displacement speed of 100 $mm.min^{-1}$ and 3 torch passes for a 5 kV voltage at 15 kHz.

The plasma-treated samples were divided into two groups. On one hand, samples were analyzed directly after plasma treatment using XPS to evaluate the extent of surface modification. On the other hand, regarding functionalization efficiency, samples were immersed in aqueous $AgNO_3$ solution (1.2 mol L^{-1}) for 90 min, at pH = 6 allowing the formation of carboxylate ions with silver as counterion ($COO\text{-}Ag^+$) [17]. Samples were then washed thoroughly with water, then dried under vacuum at 40°C, before XPS analysis. The Ag 3d XPS signal was used to determine the relative surface concentration of silver ions, which was correlated to the amount of carboxylic acid groups generated by plasma on the polymer mat.

2.4 RGD-TAMRA mimetic peptide grafting

Plasma-treated samples were, first, immersed in a 3 mg/mL EDC solution in MES buffer (0.1M, pH = 4.75)) to activate carboxylic acids. After 30 min of reaction, samples were washed two times with MES buffer and then let to react with a 2×10^{-5} M RGD-TAMRA HEPES solution at pH = 7.4 during 3h. Finally, peptide-grafted materials were washed five times with TWEEN-20 (1%) solution to remove excess of adsorbed peptides, followed by three washes with deionized water. All reactions were performed under stirring at 150 rpm, at room temperature and all materials were stored under vacuum until use.

2.5 Degradation test

The degradation rate profile of milkweed fiber mats was investigated before and after plasma treatment for 6 weeks. Milkweed samples (1 cm^3) were placed in 10 mL of MES buffered solution at pH = 4.4, in order mimic the acid-catalyzed mechanism of the ester group degradation process. The samples were removed from the solution, vacuum dried and weighted. The rate of degradation was calculated by rationing the remaining sample weight with the initial weight of the sample.

2.6 Surface characterization

2.6.1 Attenuated Total Reflectance Fourier Transformed Infrared spectroscopy (ATR-FTIR)

Spectroscopic analyses were performed to evaluate the distribution of the polymer mat components, PP, PE and milkweed, based on their respective characteristic peaks at 2950, 2848, and 1037 cm^{-1}. Images were recorded in the ATR mode on 4 cm^2 samples (1 cm thickness), using

an Agilent 620 IR microscope, equipped with a germanium-coated KBr beam splitter, a 32 × 32 focal plane array (FPA) detector cooled with liquid nitrogen and a motorized stage. In such a configuration, a spatial resolution of approx. 3.5 µm x 3.5 µm can be reached, which corresponds to the pixel size in the infrared images. This microscope assembly was attached to an Agilent 660 spectrometer. The IR microscopy images were recorded on 12 measurement points to get an overview of the sample, through the displacement of the motorized microscope stage. The 1024 spectra were simultaneously recorded between 4000 cm^{-1} and 950 cm^{-1} at a spectral resolution of 2 cm^{-1}, by co-addition and Fourier transform of 128 interferograms. Images were generated using the Agilent Pro Resolutions software (version 5.2.0.846), while spectra were analyzed using Grams 9.1 (Thermo Fisher, Waltham, MA).

Standard FTIR ATR analyses with a Split Pea attachment (Harrick Scientific) were also performed to ascertain the presence of the RGD peptide on the various investigated samples. Spectra were recorded using a deuterated lanthanum α-alanine-doped triglycine sulfate (DLaTGS) detector and a KBr beam splitter. A total of 64 interferograms were co-added and Fourier transform. The spectra are presented by comparing the relative absorbance of the 1650 cm^{-1} feature assigned to the amide I vibration of peptide bonds, therefore enabling to probe the relative amount of RGD either adsorbed of grafted on the polymer mat surface.

2.6.2 X-ray Photoelectron Spectroscopy (XPS)

The surface chemical compositions of the milkweed fibers, before and after plasma treatment, were investigated by X-ray Photoelectron Spectroscopy, using a PHI 5600-ci spectrometer (Physical Electronics, Eden Prairie, MN). A standard aluminum X-ray source (AlK_α = 1486.6 eV) was used to record survey spectra (1200-0 eV) with charge neutralization, whereas a standard magnesium source has been used for high resolution spectra without charge neutralization. The detection angle was set at 45º with respect to the normal of the surface. The curve fitting procedure with components underlying the C1s peaks was performed by means of a least-squares minimization procedure using a Gaussian–Lorentz function and a Shirley-type background. Three measurements per sample were performed within an analytical X-ray spot of 0.5 mm^2.

2.6.3 Scanning electron microscopy (SEM)

The surface morphology of milkweed fibers before and after plasma treatment was investigated by scanning electron microscope (SEM, FEI Quanta 250, Oregon, USA). SEM images were acquired with an Everhart Thornley detector (ETD) in secondary electrons mode at a voltage of 15 kV. The beam current was fixed at 45 µA. Samples were coated with Au/Pt before analysis.

2.6.4 Confocal laser scanning microscopy

Confocal laser microscopy was used to evaluate the grafting and the distribution of fluoro-tagged RGD-TAMRA peptide using a Zeiss Axio Observer Z1/7 inverted microscope (LSM 800, Oberkochen, Deutschland), equipped with a motorized stage. 3D images were acquired using Z stack (50 slices, 10 µm width) and tiles mode of the microscope software to scan a large specimen section of 1.28 x1.28 x 0.5 mm^3, at 5x magnification.

2.7 Cell culture

Commercially available MC3T3-E1 preosteoblast cells (ATCC, Canada) were grown on treated TCPS flasks in complete growth medium (alpha Minimum Essential Medium, 10% fetal bovine serum, 1% penicillin–streptomycin) (Thermo Fisher Scientific, Canada). Cells were subcultured every week using trypsin/EDTA 0.25% (Thermo Fisher Scientific, Canada), and maintained in a

humidified atmosphere with 5% CO_2 at 37°C. Milkweed samples of 1 x 1 x 1 cm^3 were sterilized in ethanol 70% solution during 1 h, rinsed three times with PBS 1X (pH = 7.4) and placed in 48-well cell culture plates. MC3T3 cells, at passage 5-7, were seeded at a density of 10^5 cells/well on untreated and peptide modified polymer mats in complete growth medium. The culture media was changed every two days. Three samples per condition were used for each experiment.

2.7.1 Cell adhesion assay

After 24h of cell culture, MC3T3-E1 preosteoblast cells were fixed with 4% formaldehyde solution for 15 min. Samples were then washed three times with PBS and stained for nuclei with 1 mg/mL DAPI solution, diluted at 0.1% (v/v) in PBS 1X. Afterward, samples were observed under confocal laser scanning microscope, using Z-stack mode (50 slices 10 μm thick), at 5x magnification. Due to the high fluorescent background of the polymer mats and the restricted depth of the microscope objective field, a large number of nuclei were out of focus on 3D images. Therefore, single plane images were stacked and z-projected using ImageJ, thus providing sharper and more realistic images.

Given that visual examination of the confocal images enabled to qualitatively evaluate the potential of the investigated materials to support cell adhesion, a quantitative assessment was performed by counting the number of adhered cells, using a hemocytometer. At 24h post-seeding, samples were transferred to new wells in order to avoid counting cells that have adhered to the bottom of the wells. Polymer mats were, first, washed two times with PBS 1X and incubated with 1 ml Trypsin/EDTA 0.25% for 8 min to detach cells. Then, 2 mL of complete growth medium were added to inhibit the trypsin effect. Samples were removed, and the cell suspension was centrifuged at 300 G during 6 min. Finally, the cell pellet was re-suspended in 1 mL of complete growth medium and cells were counted with a hemocytometer. However, cell counting was inaccurate because the cell pellets were contaminated with polymer fibers. Therefore, to overcome this problem, cells aggregated to the bottom of the wells were counted using the same procedure. It this case, a lower number of cells counted on the bottom of the well signifies that more cells are attached to the polymer mat assembly.

2.7.2 Cell viability assay

Resazurin-Reduction Assay was performed to evaluate the metabolic activity of MC3T3-E1 preosteoblast cells, at different time points (24 h, 72 h, 6 days). The assay is based on the ability of live cells to convert a non-fluorescent dye, resazurin, to a highly red fluorescent dye, resorufin. Briefly, samples were transferred to new wells and incubated with 700 µL of fresh growth medium containing 10% (v/v) resazurin solution (0.25 mg/mL) (Sigma-Aldrich, Canada) for 4 h, at 37°C and 5% CO_2. Subsequently, 100 µL of medium from each well was transferred to a clear 96-well cell culture plate and the fluorescence intensity was measured using a Fluoroskan Ascent (ThermoFisher Scientific) spectrophotometer. Excitation and emission wavelengths were set at 540 nm and 590 nm, respectively. Commercially available treated Tissue-Culture Plastic (TCP) plates were used as positive control.

2.8 Statistical analysis

Data are expressed as mean values ± standard deviation (SD). Statistical analyses were performed by one-way and two-way analysis of variance (ANOVA) for cell adhesion and viability assay, respectively, followed by Turkey's test. using. Differences were considered statistically significant for P value < 0.01, as determined by Graph-Pad Prism software.

3 RESULTS AND DISCUSSION

3.1 Mechanical characterization

The mechanical properties of the polymer mat are presented in Table 2

Table 2: Mechanical properties of the polymer mat

Direction of the applied force (degree)	Ultimate tensile strength (kPa)	Elongation at break (%)
0	13 ± 3	56 ± 8
90	8 ± 1	52 ± 2

Considering the measurement standard deviation, the polymer mat seems to be almost isotropic in terms of its mechanical characteristics with, however, a slight difference in ultimate tensile strength depending on the direction of the applied force.

3.2 Physicochemical characterization

3.2.1 Dewaxed milkweed fibers

Among all the infrared features observed in the spectrum of the mat (Figure 2a), made of 70% of milkweed, 21% of PE and 9% of PP (chemical structures given in Figure 2b), two are of particular interest because each of them is characteristic of one polymer component of the mat. First, the 1037 cm^{-1} feature is assigned to the C-O stretching mode vibration of ether bounds in cellulose, which is a major component of milkweed. Second, the presence of polyethylene in the mat is evidenced by the appearance of the 2848 cm^{-1} peak, arising from the symmetric stretching mode vibration of methylene groups ($-CH_2-$). Unfortunately, the low amount of polypropylene in the mat, and the fact that it is the core part of the core shell PE-coated PP fibers, do not enable to identify a spectroscopic feature characteristic of this polymer in the spectrum shown in Figure 2a. However, it is likely that a sufficient amount of PP would have given rise to an infrared contribution at 2950 cm^{-1}, assigned to the symmetric stretching mode of methyl groups [18].

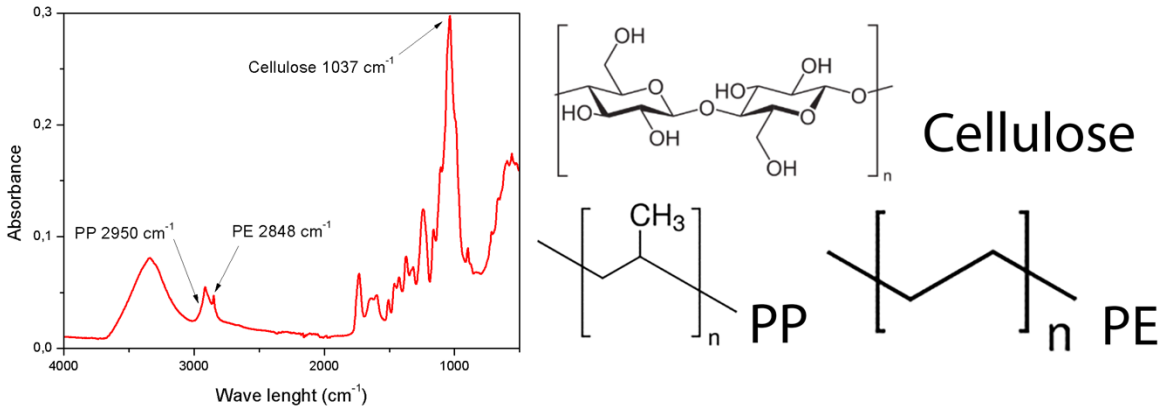

Figure 2. (Left) Typical FTIR ATR spectrum of mats made of milkweed (70%), polyethylene (21%) and polypropylene (9%), and (right) their respective chemical structure

The spatial distribution of these polymers within the mat was evaluated by IR microscopy. Images depicted in Figures 3a-c were made of 1064 pixels from which an individual spectrum can be extracted. As shown in Figure 3d, infrared spectra were taken from three different positions on the

polymer mat. From the aforementioned peak assignments, it can be concluded that position 1 is mainly composed of milkweed, while position 2 rather contains polyethylene. Despite the low polypropylene content, it is possible to highlight its presence from some of the pixels, as seen in Figure 3d. Figures 3a-c nicely enables to identify a sample area mostly containing milkweed (essentially located at the bottom of the images) and a region mainly made of a mixture of polyethylene and polypropylene. Therefore, these data demonstrated a non-homogenous distribution of the polymer mat components at the microscale level.

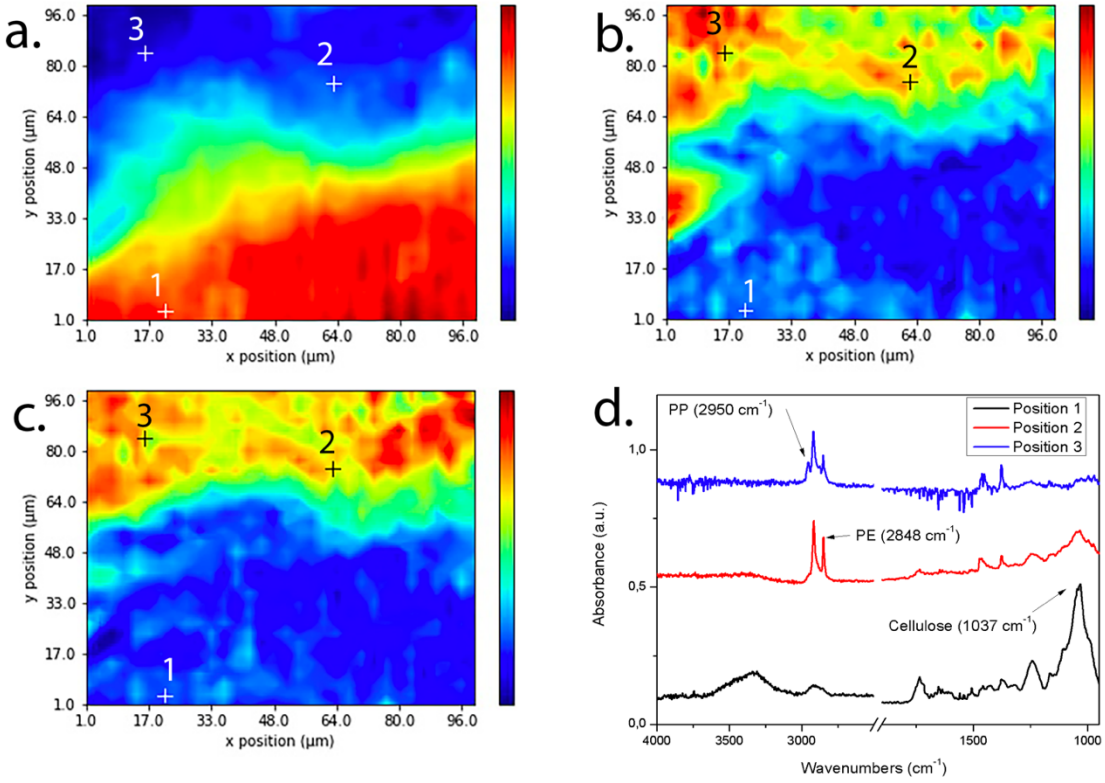

Figure 3. Images recorded by FTIR microscopy on a milkweed mat. Image recorded by measuring the absorbance of the peak centered at 1037 cm^{-1} (a), 2848 cm^{-1}(b), and. at 2950 cm^{-1} (c). (d) Spectra corresponding to the pixel marked with a cross.

To evaluate the surface chemical compositions of dewaxed polymer mats, XPS analyses were carried out on four different areas of the material, with three measurements per area. As shown in Figure 4a, the carbon and oxygen relative surface concentrations are almost identical for all polymer mat samples investigated within the experimental error. Indeed, XPS survey results showed that the polymer mat is composed of approximatively 80% of carbon and 20% of oxygen, which is very close to the theoretical values (84% carbon, 16% of oxygen, by taking into account the composition of each component and their respective amount in the mat). However, high resolution C1s data showed that the chemical environment may change depending on the analyzed area of the polymer mat surface. For instance, the proportion of cellulosic characteristic groups (structure in Figure 2b), meaning C-O groups, at 286.7 eV, and O-C-O, at 288.06 eV, may vary from 65% to 90% and 10% to 30%, respectively (Figure 4b). These bonds come mainly from cellulose and hemicellulose molecules, which are the main components of the milkweed polymers (Table 1). In addition, some spectra exhibited the C-C/C-H bond at 285.0 eV due to the presence of both PP and PE. These results are in close agreement with the infrared microscopy results, highlighting an inhomogeneous distribution of milkweed, polyethylene, and polypropylene within the polymer mat. Interestingly, slight

changes in the amount of O-C=O groups, corresponding to the peak at 290.3 eV of C1s spectrum, were noticed on the different polymer mat samples. Indeed, the proportion of O-C=O bonds, characteristic of carboxylic groups, was approximatively 5% on the surface of the polymer mat (Figure 4b).

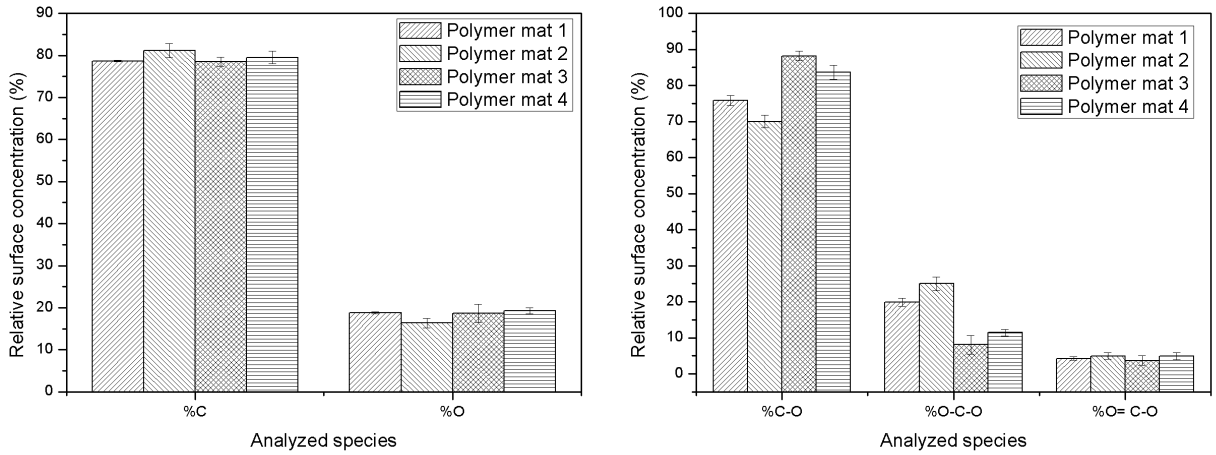

Figure 4. XPS data of four polymer mats after 24 hours of dewaxing in acetone from: a. survey analysis and b. high resolution C1s spectra

Taken together, the infrared microscopy and XPS analyses allowed to assess the chemical composition of the polymer mat surface as well as the distribution of its main components (milkweed, PE and PP).

3.2.2 Plasma-treated polymer mats

Because the overall carbon and oxygen surface concentration of the reference polymer mat was almost constant despite the observed microscale inhomogeneity (Figure 4), the XPS signal of these two elements can be used to probe the occurrence of plasma-induced surface modification. As shown by survey analyses (Figure 5a), plasma treatment on the polymer mat led to a 6-7% decrease of the carbon surface concentration, accompanied with an equivalent increase of the oxygen content.

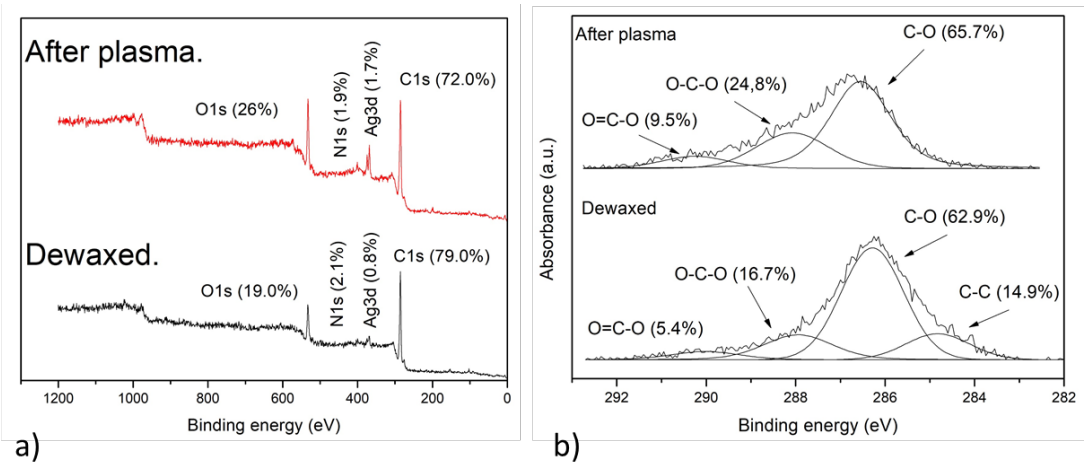

Figure 5. XPS analyses in survey mode (a) and C1s high resolution (b) on polymer mats before and after plasma treatment

Because of their important variation from one reference sample to another, C-O and O-C-O bonds are not reliable indicators of the extent of the surface modification process. However, O-C=O groups are undoubtedly a better probe, since their concentration was almost constant on the different reference polymer mat samples. As shown in high resolution spectra of C1s (Figure 5b), the amount O-C=O bonds significantly increased from 5.4% on dewaxed polymers to 9.5% on plasma-treated polymers. These observations were further corroborated by the quantification of carboxylic groups using nitric acid silver salt ($AgNO_3$), leading to carboxylate ions ($COO\text{-}Ag^+$). Therefore, the XPS signal arising from the presence of silver (Ag 3d) can be used to probe the presence of carboxylic acid residues on the material surface. The results clearly showed a two-fold increase in silver amount from 0.8% on dewaxed polymers to 1.7% on plasma-treated polymers (Figure 5a), thus suggesting that the surface functionalization of the polymer mat successfully occurred. Overall, plasma treatment allowed to create specific functional groups, required for further grafting of bioactive molecules.

SEM analyses were performed on dewaxed polymer mats, before and after plasma treatment, in order to ensure that plasma treatment did not affect the integrity of the mat structure. Images depicted in Figure 6a-b showed that dewaxed polymer mat fibers are randomly oriented, and they exhibit an elongated morphology with a fiber diameter of ≈10 micron. Following plasma treatment, some plicatures appeared along the fibers, however no serious damages were noticed over the polymer mat structure Figure (6c-d). In a previous work done by Gharehaghaji and Hayat-Davoodi, the same type of plicatures was observed on plasma-treated milkweed fibers [19]. Also, they showed a decrease in fibers length, by SEM images, which is expected to accelerate fibers degradation.

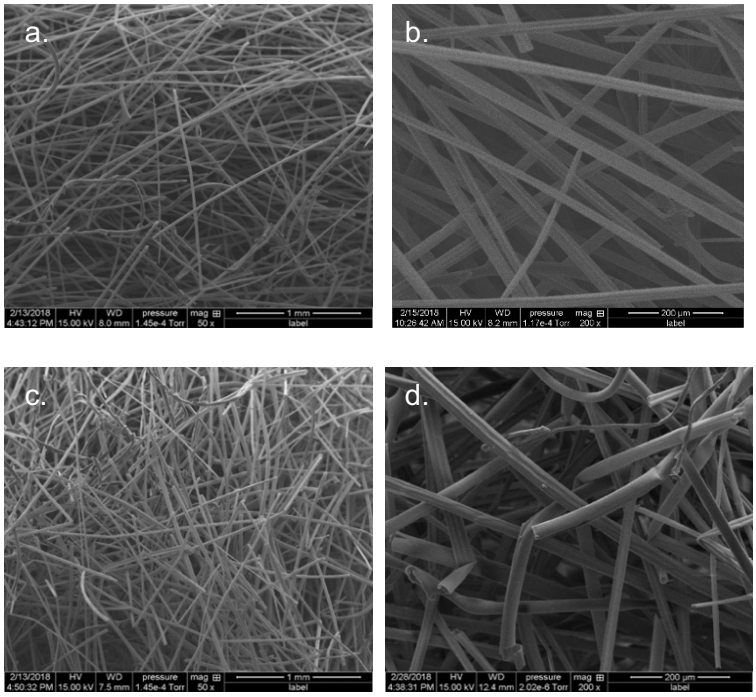

Figure 6. SEM images of the polymer mat after dewaxing. a) x50 and b) x200; polymer mat after plasma treatment. c) x50 and d) x200

3.2.3 Degradation test

Degradation tests at pH 4.4 were performed on untreated and plasma-treated polymer mats to mimic the acid-catalyzed degradation of ester groups likely to occur in the human body. The results showed a gradual mass loss in both conditions, during the investigated degradation period (6

weeks). 4.5% weight-loss in untreated polymer mats against 6% weight-loss in plasma-treated polymer mats after 6 weeks was noticed (Figure 7). These data were corroborated by SEM analyses, showing an extent of cracks on the surface of plasma-treated fibers after only one weeks in degradation solution (Figure 7). Thus, it could be concluded that the surface functionalization of the natural component of the polymer mat (milkweed) accelerates the degradation process, which is in agreement with previous studies [10]. For example, Novotna et al. showed that the oxidation does not generate a morphological modification of the fiber. On the other hand, the greater the degree of oxidation is, the more degraded the fiber.

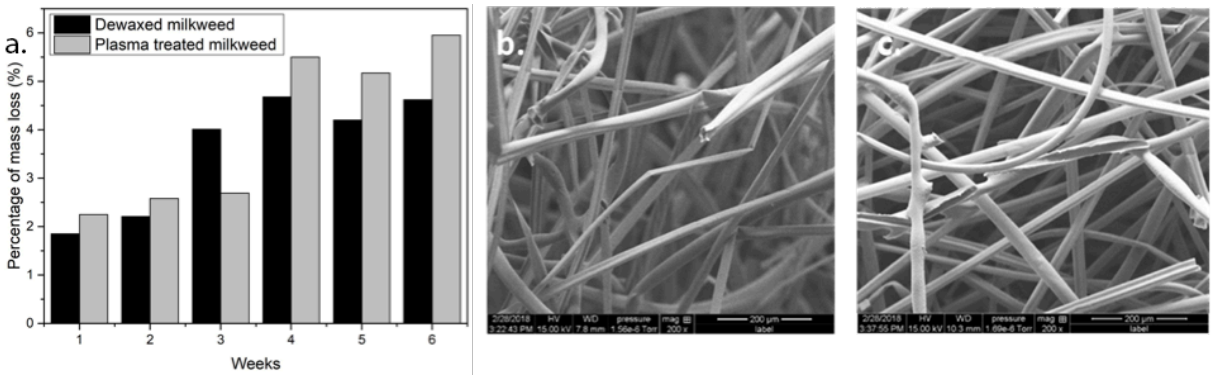

Figure 7. Percentages of mass loss of milkweed as a function of time (a); SEM images of untreated (b) and plasma-treated polymer mat (c) after7 days degradation x200.

3.2.4 Surface conjugation with mimetic peptides

As previously mentioned, peptide grafting was evidenced using a fluorotagged RGD-TAMRA peptide. This peptide is commonly used to enhance cell adhesion and spreading [20-22]. Figure 8 clearly revealed the presence of RGD peptide on the peptide-grafted polymer mats, whereas no fluorescence was detected on untreated ones.

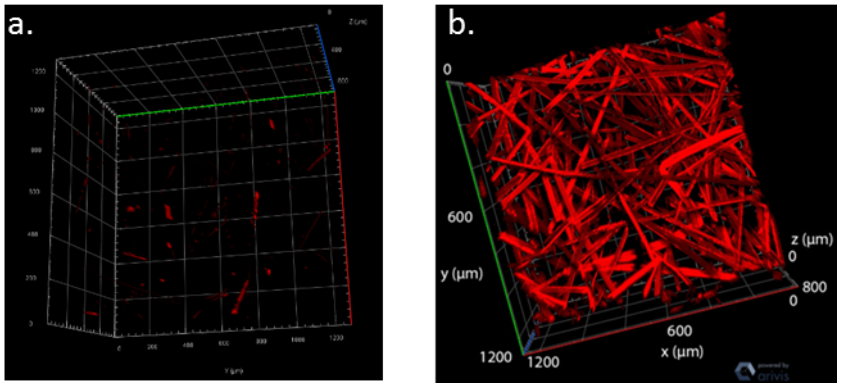

Figure 8. Confocal microscopy images of untreated (a) and RGD-TAMRA grafted milkweed (b)

These data are in concordance with FTIR results (Figure 9). In fact, compared to untreated materials, RGD containing polymer mats has led to a higher contribution of the peak at 1649 cm^{-1} (Figure 9), characteristic of peptide bonds (amide I groups) [23]. Interestingly, FTIR spectra showed that the peak intensity at 1649 cm^{-1} was higher when the carboxylic acids created on the polymer mat after plasma treatment were activated to enable further covalent conjugation of the peptide. These results suggest that the covalent grafting leads in a higher peptide density, as compared to peptide adsorption.

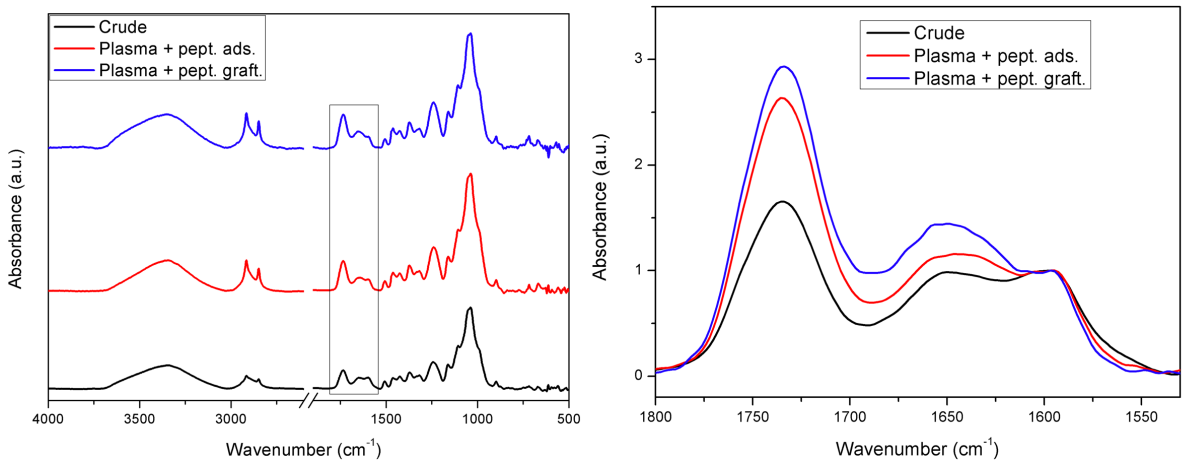

Figure 9. FTIR spectra of untreated polymer mat and of polymer mats with adsorbed or grafted RGD peptide.

3.3 Cell adhesion and metabolic activity

Preosteoblast MC3T3-E1 Cells adhesion was evaluated on untreated and RGD containing milkweed fibers after 24 h of cell culture. Fluorescent images of MC3T3 cells, labeled for nuclei with DAPI staining, showed that cells adhered on all materials. However, it seems that RGD containing milkweed fibers enhanced cell adhesion (Figure 10).

To corroborate these results, the number of cells adhered to the milkweed fibers was also estimated by indirect measurements, as described in materials and method part. These quantitative analyses revealed that the number of cells attached to the bottom of microplate wells, containing crude materials was significantly higher than the number of cells attached to the bottom of microplate wells, containing RGD-modified materials (Figure 10). This means that more cells remained on the RGD-modified milkweed fibers than untreated fibers. However, no significant difference was observed between milkweed fibers containing adsorbed or grafted RGD peptide (Figure 10). These data demonstrated that milkweed fibers allowed cell adhesion, but the presence of the peptide further enhances cell recruitment. In addition, even though the benefits of having a higher amount of immobilized peptide still have to be demonstrated, it is worth mentioning that the peptide covalent grafting enable to increase the amount of this bioactive molecule on the polymer mat sample.

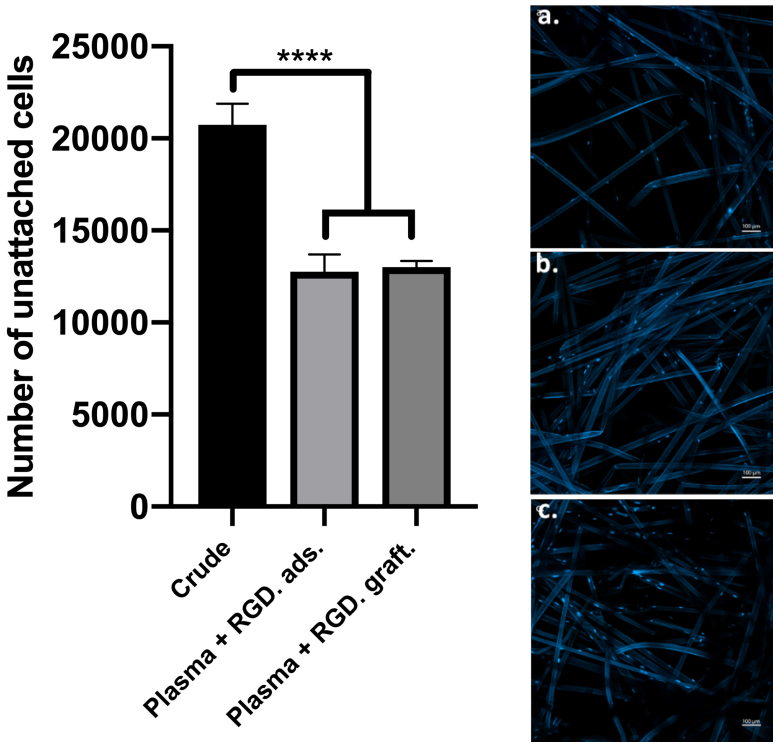

Figure 10. Fluorescence images of MC3T3-E1 preosteoblasts (nuclei stained with DAPI) cultured for 24h on: a) the polymer mat, b) plasma treated polymer mat with adsorbed RGD-TAMRA, c) plasma treated polymer mat with grafted RGD-TAMRA; The quantitative analyses of the number of cells aggregated to the bottom of microplate wells containing the untreated polymer mat (crude) and adsorbed (Plasma + RGD. Ads.) or grafted RGD peptide (Plasma + RGD. Graft.) on plasma treated polymer mat are shown on the left. *$p < 0.01$

The potential of milkweed fibers to support cell growth and viability was also evaluated over an extended period of time of up to 6 days (Figure 11). At first sight, the metabolic activity of MC3T3-E1 cells continuously increased from 24 h to 6 days, on both untreated and RGD-modified polymer mats. In addition, the metabolic activity trend was quite similar at different time points. After 24 h, cell viability was significantly higher on both grafted and adsorbed RGD polymer mats as compared to untreated ones. However, enhanced cell viability was noticed on RGD-grafted polymers, as compared to RGD-adsorbed polymers, while no significant difference was observed between RGD-grafted polymers and the positive control (TCP substrates). After 72 h and 6 days, cells cultured on RGD-grafted and RGD-adsorbed polymers exhibited similar metabolic activity, but remained significantly higher, as compared to untreated polymers. Taken together, these data highlight the biological relevance of RGD-modified milkweed fibers, owing to its capacity to recruit cells in a 3D environment, while supporting their viability and growth.

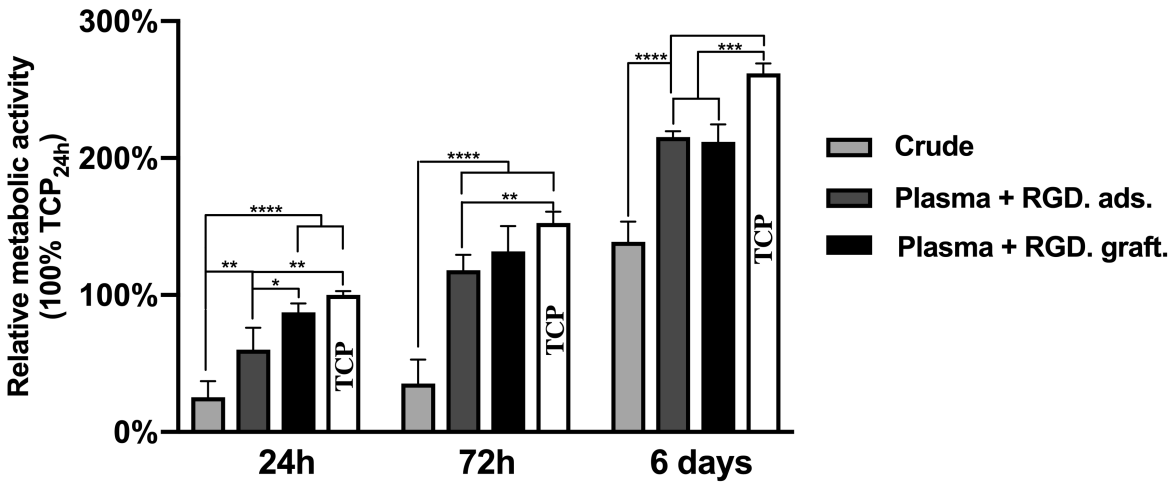

Figure 11. Relative metabolic activity of MC3T3-E1 cells determined by Resazurin-Reduction Assay on the different materials, at different periods of time. Relative measurement refers to the standardization of measured values of all conditions, in which positive control (Tissue Culture Plate (TCP), 24h) was set to 100%. * $p<0.01$

As aforementioned, milkweed fibers could be seen as potential candidates to replace silk in bone tissue engineering applications. Therefore, it is worth comparing the advantages and inconveniences of both types of fibers, even though it may be difficult due to the lack of information on the different protocols that were used to investigate both types of fibers as well as the origin of the fibers that is not always well defined. Nevertheless, from a mechanical property standpoint, the tensile strength of milkweed fibers is close to 318 MPa [24], while that of silk fibers is 600 MPa [3]. By comparison and depending on the anatomic site that is considered, the tensile strength of human bone is around 100 MPa and 120 MPa [25]. While considering the elongation at break, milkweed can be stretched up to 1.6-2.1% [24] of its initial length while this value is comprised between 20 and 30% for silk [3]. As could be intuitively expected, this value is very low for bone at 1,41% [25]. However, the interpretation of these data has to be made cautiously as it does not take into account for the final scaffold organization. For instance, in a textile such as the one used in the present study, the aforementioned mechanical properties rather refer to the moment when the textile itself breaks due to inter fiber decohesion. In this particular situation, the ultimate tensile strength for the investigated polymer mat rather ranges between 3 kPa and 5 kPa with an elongation at break between 50% and 65% (while considering the standard deviations), depending on the direction at which the test was performed. In a context of regenerative medicine, this highlights the fact that one should not only try to match the mechanical properties of the biological tissue to be substituted with that of the raw substitution material but should also consider the mechanical properties of this substitution material once integrated in a 3D textile structure.

On the chemistry side, milkweed is a cellulose-based material which, by nature, cannot be degraded by classical physiological process such as hydrolysis or enzymatic degradation. However, this drawback can be circumvented by applying a surface modification treatment on the fiber surface which leads to the formation of carboxylic acid residues that could be hydrolyzed to initiate the degradation process [10]. On the other hand, silk is a protein and accordingly could be degraded by classical physiological mechanisms [3].

Finally, the ease of fiber production also has to be taken into account. Milkweed naturally grows in environments that seem hostile to the establishment of cultivated plants such as devalued farmland, edges of fields, or ditches. In addition, the harvesting of milkweed fibers is greatly facilitated by modern farming technologies. In the case of silk extracted from the silkworm (Bombix mori), there are problems of characterization of the fiber due to a variable extraction of sericin, which

is the wax that naturally covers the silk. Moreover, the process of silk dewaxing greatly modifies its physicochemical properties. For its part, spider silk is much cleaner but the production that can be obtained from this source is much too low to hope to valorize it in the form of textile in general, and biomedical textile in particular [26, 27]. Finally, from an economical perspective, one kilogram of milkweed fibers costs between one and five US dollars [28] while the price for an equivalent amount of silk is rather of 55 US dollars [29].

It also worth mentioning the state-of-the-art related to scaffold for bone tissue engineering made of silk. Indeed, engineering such a scaffold requires putting together several knowledges and know-how in terms of textile structure and porosity [30-31], control over the silk protein structure [32], surface modification [33-39], integration as a part of a composite material [40-41], blending with biodegradable polymers [26, 42-43], or therapeutic molecule inclusion [44-47]. The present publication definitely shows that some of these improvements could also be done on a milkweed-based scaffold. That said, it is also clear that some research still has to be done to reach a level of achievement similar to that of silk-based scaffolds.

All in all, milkweed fiber could be an interesting alternative to silk for bone tissue engineering applications, as its mechanical properties are closer to that of the tissues to be repaired. In addition, milkweed can be produced in high quantity at low cost. However, the focus will have to be put on the surface modification of the fiber to reach degradation kinetics similar to that of silk. In addition, solutions will have to be put forward to get cohesive milkweed fiber mats without the presence of synthetic polymers, to take full advantage of milkweed fiber potential for degradation.

4 CONCLUSIONS

A polymer mat made of milkweed, polyethylene, and polypropylene has been investigated as a potential scaffold for bone regeneration. In this context, an atmospheric plasma treatment was applied on the milkweed fiber to create specific chemical groups on the surface to enable the conjugation of a cell adhesion peptide (RGD) and promote its biodegradation through acid-catalyzed scission of ester groups generated by the plasma treatment. First, we evidenced that plasma treatment increased the number of carboxylic acid groups on the fiber, while breaking down the polymer chains, which is expected to accelerate its degradation. From a biological point of view, the results demonstrated that preosteoblast cells are able to interact with the polymer, and that the conjugation of the milkweed fiber with RGD peptide significantly enhances cell adhesion. Therefore, this work provides new insights into the potential of the milkweed fiber as a biodegradable scaffold for bone tissue engineering.

ACKNOWLEDGEMENTS

This work was supported by the Centre Québécois sur les Matériaux Fonctionnels (CQMF), and the National Science and Engineering Research Council (NSERC) of Canada.

REFERENCES

[1] Gassling, V.; Hedderich, J.; Açil, Y.; Purcz, N.; Wiltfang, J.; Douglas, T. Comparison of Platelet Rich Fibrin and Collagen as Osteoblast-Seeded Scaffolds for Bone Tissue Engineering Applications. Clin. Oral Implants Res. 2013, 24, 320–328. https://doi.org/10.1111/j.1600-0501.2011.02333.x.

[2] Hutmacher, D. W. Scaffolds in Tissue Engineering Bone and Cartilage. Biomaterials 2000, 21, 2529–2543. https://doi.org/10.1016/S0142-9612(00)00121-6.

[3] Bhattacharjee, P.; Kundu, B.; Naskar, D.; Kim, H. W.; Maiti, T. K.; Bhattacharya, D.; Kundu, S. C. Silk Scaffolds in Bone Tissue Engineering: An Overview. Acta Biomater. 2017, 63, 1–17. https://doi.org/10.1016/j.actbio.2017.09.027.

[4] Meinel, L.; Hofmann, S.; Karageorgiou, V.; Kirker-Head, C.; McCool, J.; Gronowicz, G.; Zichner, L.; Langer, R.; Vunjak-Novakovic, G.; Kaplan, D. L. The Inflammatory Responses to Silk Films in Vitro and in Vivo. Biomaterials 2005, 26, 147–155. https://doi.org/10.1016/j.biomaterials.2004.02.047.
[5] Vepari, C.; Kaplan, D. L. Silk as a Biomaterial. Prog. Polym. Sci. 2007, 32, 991–1007. https://doi.org/10.1016/j.progpolymsci.2007.05.013.
[6] Leprince, J.-M. La soie d'Amérique, rempart contre les fuites d'hydrocarbures et amie du papillon monarque http://ici.radio-canada.ca/nouvelle/696242/soie-amerique-asclepiade-absorbant-petrole-survie-monarque (accessed Sep 27, 2017).
[7] Choi, H. M.; Cloud, R. M. Natural Sorbents in Oil Spill Cleanup. Environ. Sci. Technol. 1992, 26, 772–776.
[8] Liu, X.; Sun, Q.; Wang, H.; Zhang, L.; Wang, J. Microspheres of Corn Protein, Zein, for an Ivermectin Drug Delivery System. Biomaterials 2005, 26, 109–115. https://doi.org/10.1016/j.biomaterials.2004.02.013.
[9] Cheatham, S.; Johnston, M.; Marshall, L.; The Useful Wild Plants of Texas, the Southeastern and Southwestern United States, the Southern Plains, and Northern Mexico. Austin, TX: Useful Wild Plants, Inc; 2000; Vol, 2.
[10] K. Novotna, P. Havelka, T. Sopuch, K. Kolarova, V. Vosmanska, V. Lisa, V. Svorcik, and L. Bacakova, "Cellulose-based materials as scaffolds for tissue engineering," Cellulose, vol. 20, no. 5, pp. 2263–2278, 2013.
[11] Bellis, S. L. Advantages of RGD Peptides for Directing Cell Association with Biomaterials. Biomaterials 2012, 32, 4205–4210.
[12] Sarra-Bournet, C.; Turgeon, S.; Mantovani, D.; Laroche, G. Comparison of Atmospheric-Pressure Plasma versus Low-Pressure RF Plasma for Surface Functionalization of PTFE for Biomedical Applications. Plasma Process. Polym. 2006, 3 (6–7), 506–515.
[13] Davis, R.; El-Shafei, A.; Hauser, P. Use of Atmospheric Pressure Plasma to Confer Durable Water Repellent Functionality and Antimicrobial Functionality on Cotton/Polyester Blend. Surf. Coatings Technol. 2011, 205 (20), 4791–4797.
[14] Wang, R.; Zhang, C.; Liu, X.; Xie, Q.; Yan, P.; Shao, T. Microsecond Pulse Driven Ar/CF4 Plasma Jet for Polymethylmethacrylate Surface Modification at Atmospheric Pressure. Appl. Surf. Sci. 2015, 328, 509–515.
[15] Taha, I.; Ziegmann, G. A Comparison of Mechanical Properties of Natural Fiber Filled Biodegradable and Polyolefin Polymers. J. Compos. Mater. 2006, 40 (21), 1933–1946.
[16] Richard, C.; Cousin, P.; Foruzanmehr, Mr.; Elkoun, S.; Robert, M. Characterization of Extracted Components of Milkweed Floss Fiber. Sep. Sci. Technol. 2018.
[17] Crombez, M.; Chevallier, P.; C.-Gaudreault, R.; Petitclerc, E.; Mantovani, D.; Laroche, G. Improving Arterial Prosthesis Neo-Endothelialization: Application of a Proactive VEGF Construct onto PTFE Surfaces. Biomaterials 2005, 26, 7402–7409.
[18] Guimond, S.; Radu, I.; Czeremuszkin, G.; Carlsson, D. J.; Wertheimer, M. R. Biaxially Oriented Polypropylene (BOPP) Surface Modification by Nitrogen Atmospheric Pressure Glow Discharge (APGD) and by Air Corona. Plasmas Polym. 2002, 7 (1), 71–88.
[19] Gharehaghaji, A.; Hayat-Davoodi, S. Mechanical Damage to Estabragh Fibers in the Production of Thermobonded Layers. J Appl Polym Sci 2008, 109, 3062–3069.
[20] Porté-Durrieu, M. C.; Guillemot, F.; Pallu, S.; Labrugère, C.; Brouillaud, B.; Bareille, R.; Amédée, J.; Barthe, N.; Dard, M.; Baquey, C. Cyclo-(DfKRG) Peptide Grafting onto Ti-6Al-4V: Physical Characterization and Interest towards Human Osteoprogenitor Cells Adhesion. Biomaterials 2004, 25, 4837–4846.
[21] Hoesli, C. A.; Garnier, A.; Juneau, P. M.; Chevallier, P.; Duchesne, C.; Laroche, G. A Fluorophore-Tagged RGD Peptide to Control Endothelial Cell Adhesion to Micropatterned Surfaces. Biomaterials 2014, 35, 879–890.

[22] Zhang, H.; Lin, C. Y.; Hollister, S. J. The Interaction between Bone Marrow Stromal Cells and RGD-Modified Three-Dimensional Porous Polycaprolactone Scaffolds. Biomaterials 2009, 30, 4063–4069.
[23] Boonsongrit, Y.; Mueller, B. W.; Mitrevej, A. Characterization of Drug-Chitosan Interaction by 1H NMR, FTIR and Isothermal Titration Calorimetry. Eur. J. Pharm. Biopharm. 2008, 69, 388–395.
[24] Hassanzadeh, S.; Hasani, H. A Review on Milkweed Fiber Properties as High-Potential Raw Material in Textile Applications. J. Ind. Text. 2017, 46, 1412-1436.
[25] Pal, S. Design of Artificial Human Joints & Organs, Springer: Boston, 2014.
[26] Altman, G.H.; Diaz, F.; Jakuba, C.; Calabro, T.; Horan, R.L.; Chen, J.; Lu, H.; Richmond, J.; Kaplan, D.L. Silk-Based Biomaterials, Biomaterials 2003, 24, 401-416.
[27] Melke, J.; Midha S.; Ghosh, S.; Ito, K.; Hoffmann, S. Silk Fibroin as Biomaterial for Bone Tissue Engineering", Acta Biomater. 2016, 31, 1-16.
[28] Nehring, J. The potential of milkweed floss as a natural fiber in the textile industry, J. Undergrad. Res. https://kuscholarworks.ku.edu/bitstream/handle/1808/15034/Nehring_jur14.pdf?sequence=1&isAllowed=y.
[29] EmergingTextiles.com. http://www.emergingtextiles.com/?q=art&s=170130-silk-market-price&r=free&i=samplearticle (accessed on January 25th, 2019).
[30] Jin, H.-J.; Chen, J.; Karageorgiou, V.; Altman, G.H.; Kaplan, D.L. Human bone marrow stromal cell responses on electrospun silk fibroin mats. Biomaterials 2004, 25, 1039–1047.
[31] Ma, P.X.; Zhang, R. Synthetic nano-scale fibrous extracellular matrix. J. Biomed. Mater. Res. 1999, 46, 60–72.
[32] Mandal, B.B.; Grinberg, A.; Gil, E.S.; Panilaitis, B.; Kaplan, D.L. High-strength silk protein scaffolds for bone repair. PNAS 2012, 109, 7699–7704.
[33] Cao, H.; Chen, X.; Yao, J.; Shao, Z. Fabrication of an alternative regenerated silk fibroin nanofiber and carbonated hydroxyapatite multilayered composite via layer-by-layer. J. Mater. Sci. Mater. Med. 2013, 48, 150–155.
[34] Zhao, J.; Zhang, Z.; Wang, S.; Sun, X.; Zhang, X.; Chen, J.; Kaplan, D.L.; Jiang, X.; Apatite coated silk fibroin scaffolds to healing mandibular border defects in canines. Bone 2009, 45, 517–527.
[35] Kim, H.J.; Kim, U.-J.; Kim, H.S.; Li, C.; Wada, M.; Leisk, G.G.; Kaplan, D.L. Bone tissue engineering with premineralized silk scaffolds. Bone 2008, 42, 1226– 1234.
[36] Tanaka, T.; Hirose, M.; Kotobuki, N.; Ohgushi, H.; Furuzono, T.; Sato, J. Nano-scaled hydroxyapatite/silk fibroin sheets support osteogenic differentiation of rat bone marrow mesenchymal cells. Mater. Sci. Eng. C Mater. Biol. Appl. 2007, 27, 817–823.
[37] Bhattacharjee, P.; Naskar, D.; Maiti, T.K.; Bhattacharya, D. Kundu, S.C. Non- mulberry silk fibroin grafted poly (e-caprolactone) nanofibrous scaffolds mineralized by electrodeposition: an optimal delivery system for growth factors to enhance bone regeneration. RSC Adv. 2016, 6, 26835–26855.
[38] Li, J.J.; Gil, E.S.; Hayden, R.S.; Li, C.; Roohani-Esfahani, S.-I.; Kaplan, D.L.; Zreiqat, H. Multiple silk coatings on biphasic calcium phosphate scaffolds: effect on physical and mechanical properties and in vitro osteogenic response of human mesenchymal stem cells. Biomacromolecules 2013, 14, 2179–2188.
[39] Jiang, J.; Hao, W.; Li, Y.; Yao, J.; Shao, Z.; Li, H.; Yang, J.; Chen, S. Hydroxyapatite/ regenerated silk fibroin scaffold-enhanced osteoinductivity and osteoconductivity of bone marrow-derived mesenchymal stromal cells. Biotechnol. Lett. 2013, 35, 657–661.
[40] Jiang, X.; Zhao, J.; Wang, S.; Sun, X.; Zhang, X.; Chen, J.; Kaplan, D.L.; Zhang, Z. Mandibular repair in rats with premineralized silk scaffolds and BMP-2- modified bMSCs. Biomaterials 2009, 30, 4522–4532.

[41] Chen, L.; Hu, J.; Ran, J.; Shen, X.; Tong, H. Preparation and evaluation of collagen- silk fibroin/hydroxyapatite nanocomposites for bone tissue engineering. Int. J. Biol. Macromol. 2014, 65, 1–7.
[42] Roohani-Esfahani, S.I.; Lu, Z.F.; Li, J.J.; Ellis-Behnke, R.; Kaplan, D.L.; Zreiqat, H. Effect of self-assembled nanofibrous silk/polycaprolactone layer on the osteoconductivity and mechanical properties of biphasic calcium phosphate scaffolds. Acta Biomater. 2012, 8, 302–312.
[43] Gui-Bo, Y.; Zhang, Z.; Shu-Dong, W.; De-Bing, S.; Zhi-Hui, D.; Wei-Guo, F. Study of the electrospun PLA/silk fibroin-gelatin composite nanofibrous scaffold for tissue engineering. J. Biomed. Mater. Res. 2010, A 93, 158–163.
[44] Lee, E.-H.; Kim, J.-Y.; Kweon, H.Y.; Jo, Y.-Y.; Min, S.-K.; Park, Y.-W.; Choi, J.-Y.; Kim, S.-G. A combination graft of low-molecular-weight silk fibroin with Choukroun platelet-rich fibrin for rabbit calvarial defect. Oral Surg. Oral Med. Oral Pathol. Oral Radiol. Endod. 2010, 109, e33–e38.
[45] Damoulis, P.D.; Drakos, D.E.; Gagari, E.; Kaplan, D.L. Osteogenic differentiation of human mesenchymal bone marrow cells in silk scaffolds is regulated by nitric oxide. Ann. N. Y. Acad. Sci. 2007, 1117, 367–376.
[46] Zhang, Y.; Fan, W.; Nothdurft, L.; Wu, C.; Zhou, Y.; Crawford, R.; Xiao, Y. In vitro and in vivo evaluation of adenovirus combined silk fibroin scaffolds for bone morphogenetic protein-7 gene delivery. Tissue Eng. Part C 2011, 17, 789– 797.
[47] Wenk, E.; Meinel, A.J.; Wildy, S.; Merkle, H.P.; Meinel, L. Microporous silk fibroin scaffolds embedding PLGA microparticles for controlled growth factor delivery in tissue engineering. Biomaterials 2009, 30, 2571–2581.